Antibonding ground state of adatom molecules in bulk Dirac semimetals

Y. Marques,[1] A. E. Obispo,[2,3] L. S. Ricco,[1] M. de Souza,[2] I. A. Shelykh,[4,5] and A. C. Seridonio[1,2]

[1]*Departamento de Física e Química, Unesp-Universidade Estadual Paulista, 15385-000 Ilha Solteira, São Paulo, Brazil*
[2]*Departamento de Física, IGCE, Unesp-Universidade Estadual Paulista, 13506-900 Rio Claro, São Paulo, Brazil*
[3]*Departamento de Física, Universidade Federal do Maranhão, 65080-805 São Luís, Maranhão, Brazil*
[4]*Science Institute, University of Iceland, Dunhagi-3, IS-107 Reykjavik, Iceland*
[5]*ITMO University, St. Petersburg 197101, Russia*

The ground state of the diatomic molecules in nature is inevitably bonding, and its first excited state is antibonding. We demonstrate theoretically that, for a pair of distant adatoms placed buried in three-dimensional-Dirac semimetals, this natural order of the states can be reversed and an antibonding ground state occurs at the lowest energy of the so-called bound states in the continuum. We propose an experimental protocol with the use of a scanning tunneling microscope tip to visualize the topographic map of the local density of states on the surface of the system to reveal the emerging physics.

Introduction. Three-dimensional Dirac semimetals (3D-DSMs), such as cadmium arsenide (Cd_3As_2) and Na_3Bi [1–5] represent a novel class of functional materials constituting 3D analogs of gapless graphene [6–8]. The band structure of 3D semimetals contains the set of the so-called Dirac points in which conduction and valence bands touch and effective mass becomes zero. Around these points the dispersion of quasi-particles corresponds to those of massless relativistic Dirac particles which result in a series of unusual properties of these materials, such as linear magnetoresistance, unprecedented Shubnikov–de Haas oscillations, and ultrahigh carrier mobility [9–11].

In this Rapid Communication, we predict one more interesting feature of such materials. Namely, if we consider a buried pair of distant adatoms in the bulk of a 3D-DSM as depicted in Fig. 1, the ground state of this molecular system formed from bound states in the continuum (BICs) of the adatoms [12–14] will be characterized by an antibonding-type orbital. This differs from the natural order in diatomic molecules where the ground state is of bonding type in the vast majority of cases and the formation of the antibonding ground state until now was reported only in systems of artificially fabricated InAs and Ge/Si *p*-type quantum dots for certain values of the interdot separations [15,16]. The behavior we report is a unique effect arising from long-range correlations between distant adatoms mediated by bulk fermions in 3D-DSMs. To detect the predicted effect, we propose to use the experimental approach developed in Ref. [17] for imaging isodensity contours of molecular states by a STM tip as outlined in Fig. 1.

The Model. For theoretical analysis of two adatoms buried inside a 3D-DSM as depicted in Fig. 1 we employ an Anderson-like Hamiltonian [18–20],

$$\mathcal{H}_{\text{T}} = \mathcal{H}_0 + \mathcal{H}_{\text{d}} + \mathcal{H}_V, \tag{1}$$

in which the effective low-energy term describing the 3D-DSM is given by

$$\mathcal{H}_0 = \sum_{\mathbf{k},\tau} \psi_\tau^\dagger(\mathbf{k}) h_\tau(\mathbf{k}) \psi_\tau(\mathbf{k}), \tag{2}$$

where $\psi_\tau^\dagger(\mathbf{k}) = (c_{\mathbf{k}\tau\uparrow}^\dagger \quad c_{\mathbf{k}\tau\downarrow}^\dagger)$ is a spinor with fermionic operators $c_{\mathbf{k}\tau\sigma}^\dagger$ ($c_{\mathbf{k}\tau\sigma}$) for creation (annihilation) of electrons in quantum states labeled by the wave-vector $\mathbf{k}$, spin σ, and chirality $\tau = \pm$, and

$$h_\tau(\mathbf{k}) = v_F \tau (k_x \sigma_x + k_y \sigma_y + k_z \sigma_z), \tag{3}$$

where σ_i accounts for the Pauli matrices and v_F is the Fermi velocity.

The term,

$$\mathcal{H}_{\text{d}} = \sum_{j\sigma} \varepsilon_{d_{j\sigma}} d_{j\sigma}^\dagger d_{j\sigma} + \sum_j U_j n_{d_{j\uparrow}} n_{d_{j\downarrow}} \tag{4}$$

describes the buried adatoms ($j = 1,2$), where $n_{d_{j\sigma}} = d_{j\sigma}^\dagger d_{j\sigma}$, $d_{j\sigma}^\dagger$ ($d_{j\sigma}$) creates (annihilates) an electron with spin σ in state $\varepsilon_{d_{j\sigma}}$, and U_j is the on-site Coulomb repulsion.

$\mathcal{H}_V$ accounts for the hybridization between the adatoms and the host,

$$\mathcal{H}_V = \sum_{j\mathbf{k}\tau} \hat{d}_j^\dagger \hat{V}_{j\mathbf{k}} \psi_\tau(\mathbf{k}) + \text{H.c.}, \tag{5}$$

where $\hat{d}_j^\dagger = (d_{j\uparrow}^\dagger \quad d_{j\downarrow}^\dagger)$ and

$$\hat{V}_{j\mathbf{k}} = \begin{pmatrix} V_{j\mathbf{k}} & 0 \\ 0 & V_{j\mathbf{k}} \end{pmatrix} \tag{6}$$

is a hybridization matrix. We assume that both adatoms are coupled equally to the 3D-DSM in such a way that $V_{j\mathbf{k}} = \frac{v_0}{\sqrt{\mathcal{N}}} e^{i\mathbf{k}\cdot\mathbf{R}_j}$ in which $\mathcal{N}$ gives the total number of states in the band structure and $\mathbf{R}_j$ corresponds to the positions of the buried adatoms.

To explore the effects induced by the adatoms, we focus on the LDOS of the system given by

$$\text{LDOS}(\varepsilon, \mathbf{R}_m) = -\frac{1}{\pi} \text{Im} \left[\sum_\sigma \tilde{\mathcal{G}}_\sigma(\varepsilon, \mathbf{R}_m) \right], \tag{7}$$

where

$$\tilde{\mathcal{G}}_\sigma(\varepsilon, \mathbf{R}_m) = \frac{1}{\mathcal{N}} \sum_{\mathbf{k}\mathbf{q}} \sum_{\tau\tau'} e^{-i\mathbf{k}\cdot\mathbf{R}_m} e^{i\mathbf{q}\cdot\mathbf{R}_m} \tilde{\mathcal{G}}_{c_{\mathbf{k}\tau\sigma} c_{\mathbf{q}\tau'\sigma}} \tag{8}$$
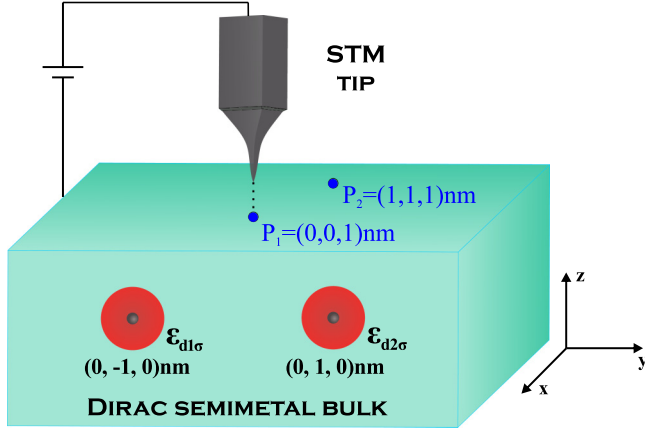
FIG. 1. Sketch of the setup proposed: two adatoms with energy levels $\varepsilon_{d_{1\sigma}}$ and $\varepsilon_{d_{2\sigma}}$, buried in a 3D-DSM at positions $\mathbf{R}_1 = (0, -1, 0)$ and $\mathbf{R}_2 = (0, 1, 0)$ nm, respectively. P_1 and P_2 on top of the host represent sites in which the local density of states (LDOS) are probed by a scanning tunneling microscope (STM) tip.

is the system's Green's function in energy domain ε at the STM-tip position $\mathbf{R}_m$. By applying the equation-of-motion (EOM) procedure [13,21] for the previous equation, we find

$$\tilde{\mathcal{G}}_{c_{\mathbf{k}\tau\sigma} c_{\mathbf{q}\tau'\sigma}} = \frac{(\varepsilon \pm \hbar v_F \tau k_z)\delta_{\mathbf{k}\mathbf{q}}\delta_{\tau\tau'}}{\varepsilon^2 - (\tau \hbar v_F k)^2}$$
$$+ \frac{(\varepsilon \pm \hbar v_F \tau k_z)\sum_j V_{j\mathbf{k}}}{\varepsilon^2 - (\tau \hbar v_F k)^2}\tilde{\mathcal{G}}_{d_{j\sigma} c_{\mathbf{q}\tau'\sigma}}$$
$$+ \frac{(\hbar v_F \tau k_-)\sum_j V_{j\mathbf{k}}}{\varepsilon^2 - (\tau \hbar v_F k)^2}\tilde{\mathcal{G}}_{d_{j\bar{\sigma}} c_{\mathbf{q}\tau'\sigma}}, \quad (9)$$

where $\pm$ stands for $\sigma =\uparrow, \downarrow$, respectively, with $\bar{\sigma} = -\sigma$ and $k_{\pm} = k_x \pm i k_y$. To finish the LDOS evaluation, we first perform the summation over τ and τ', which gives

$$\tilde{\mathcal{G}}^{\text{full}}_{c_{\mathbf{k}\sigma} c_{\mathbf{q}\sigma}} = \frac{2\varepsilon\delta_{\mathbf{k}\mathbf{q}}}{\varepsilon^2 - (\hbar v_F k)^2} + \frac{2\varepsilon \sum_j V_{j\mathbf{k}}}{\varepsilon^2 - (\hbar v_F k)^2}\sum_{\tau'}\tilde{\mathcal{G}}_{d_{j\sigma} c_{\mathbf{q}\tau'\sigma}}, \quad (10)$$

where we defined $\tilde{\mathcal{G}}^{\text{full}}_{AB} \equiv \sum_{\tau\tau'} \tilde{\mathcal{G}}_{AB}$. By applying the EOM method for the mixed Green's function $\sum_{\tau'} \tilde{\mathcal{G}}_{d_{j\sigma} c_{\mathbf{q}\tau'\sigma}}$, we determine

$$\sum_{\tau'}\tilde{\mathcal{G}}_{d_{j\sigma} c_{\mathbf{q}\tau'\sigma}} = \frac{2\varepsilon \sum_l V^*_{l\mathbf{q}}}{\varepsilon^2 - (\hbar v_F q)^2}\tilde{\mathcal{G}}_{d_{j\sigma} d_{l\sigma}}, \quad (11)$$

and consequently,

$$\tilde{\mathcal{G}}_\sigma(\varepsilon, \mathbf{R}_m) = \frac{1}{\mathcal{N}}\sum_{\mathbf{k}\mathbf{q}}\frac{2\varepsilon\delta_{\mathbf{k}\mathbf{q}}}{\varepsilon^2 - (\hbar v_F k)^2} + \frac{1}{v_0^2}\sum_{jl}\tilde{\mathcal{G}}_{d_{j\sigma} d_{l\sigma}}$$
$$\times \Sigma(\mathbf{R}_{mj})\Sigma(\mathbf{R}_{lm}), \quad (12)$$

in which $\mathbf{R}_{mj} = \mathbf{R}_m - \mathbf{R}_j$, $\mathbf{R}_{mj} = -\mathbf{R}_{jm}$ and

$$\Sigma(\mathbf{R}_{mj}) = \frac{2v_0^2}{\mathcal{N}}\sum_{\mathbf{k}}\frac{\varepsilon e^{i\mathbf{k}\cdot\mathbf{R}_{mj}}}{\varepsilon^2 - (\hbar v_F k)^2} \quad (13)$$

gives the noninteracting self-energy. After performing the sum over $\mathbf{k}$ and introducing the energy cutoff D as the band

half-width of the 3D-DSM, we get

$$\Sigma(\mathbf{R}_{mj}) = -\frac{3\pi v_0^2 \varepsilon}{D^3}\frac{\hbar v_F}{|R_{mj}|}\exp\left(\frac{i|R_{mj}|\varepsilon}{\hbar v_F}\right). \quad (14)$$

This equation holds in the domain $\frac{|R_{mj}|\varepsilon}{\hbar v_F} \gg 1$, i.e, for long-range positions. Particularly at the adatom site, the self-energy reads

$$\Sigma(0) = -\frac{6\varepsilon v_0^2}{D^2}\left(1 - \frac{\varepsilon}{2D}\ln\left|\frac{D+\varepsilon}{D-\varepsilon}\right|\right) - i\pi\mathcal{D}_0 v_0^2, \quad (15)$$

with 3D-DSM DOS determined by $\mathcal{D}_0 = \frac{\Omega}{\pi^2 \hbar^3 v_F^3 \mathcal{N}}\varepsilon^2 = \frac{3\varepsilon^2}{D^3}$, which exhibits quadratic scaling on energy in agreement with Ref. [22].

As a result the LDOS of the system is given by

$$\text{LDOS}(\varepsilon, \mathbf{R}_m) = 2\mathcal{D}_0 + \sum_{jl}\Delta\text{LDOS}_{jl}(\mathbf{R}_m), \quad (16)$$

where

$$\Delta\text{LDOS}_{jl}(\mathbf{R}_m) = -\frac{1}{\pi v_0^2}\sum_\sigma \text{Im}\left\{\Sigma(\mathbf{R}_{mj})\tilde{\mathcal{G}}_{d_{j\sigma} d_{l\sigma}}\Sigma(\mathbf{R}_{lm})\right\} \quad (17)$$

stands for the term induced by the presence of the buried adatoms. The diagonal terms in it with $j = l$ describe the electronic waves scattered by individual adatoms, whereas mixing terms with $j \neq l$ correspond to the waves that travel back and forth between two adatoms. The aforementioned quantities are of major importance for the appearance of the so-called BICs, which emerge when ΔLDOS_{jl} for $j \neq l$ contribute with the Fano antiresonance [23,24] phase shifted by π with respect to the resonance arising from ΔLDOS_{jj}. Noteworthy, both quantities depend on the DOS of the adatoms,

$$\text{DOS}_{jl} = -\frac{1}{\pi}\text{Im}\left(\sum_\sigma \tilde{\mathcal{G}}_{d_{j\sigma} d_{l\sigma}}\right). \quad (18)$$

To evaluate functions $\tilde{\mathcal{G}}_{d_{j\sigma} d_{l\sigma}}$, we start employing the EOM approach which gives

$$[\varepsilon - \varepsilon_{d_{j\sigma}} - \Sigma(0)]\tilde{\mathcal{G}}_{d_{j\sigma} d_{l\sigma}} = \delta_{jl} + U_j\tilde{\mathcal{G}}_{d_{j\sigma} n_{d_{j\bar{\sigma}}} d_{l\sigma}}$$
$$+ \Sigma(\mathbf{R}_{j\bar{j}})\tilde{\mathcal{G}}_{d_{\bar{j}\sigma} d_{l\sigma}}, \quad (19)$$

where $\bar{j} = 1, 2$ when $j = 2, 1$. In this expression, $\tilde{\mathcal{G}}_{d_{j\sigma} n_{d_{j\bar{\sigma}}} d_{l\sigma}}$ stands for the two-particle Green's function, which yields

$$(\varepsilon - \varepsilon_{d_{j\sigma}} - U_j)\tilde{\mathcal{G}}_{d_{j\sigma} n_{d_{j\bar{\sigma}}} d_{l\sigma}}$$
$$= \delta_{jl}\langle n_{d_{j\bar{\sigma}}}\rangle + \sum_{\mathbf{k}\tau}V_{j\mathbf{k}}\left[\tilde{\mathcal{G}}_{d^\dagger_{j\bar{\sigma}} c_{\mathbf{k}\tau\bar{\sigma}} d_{j\sigma}, d_{l\sigma}} + \tilde{\mathcal{G}}_{c_{\mathbf{k}\tau\sigma} d^\dagger_{j\bar{\sigma}} d_{j\bar{\sigma}}, d_{l\sigma}}\right.$$
$$\left. - V_{j\mathbf{k}}\tilde{\mathcal{G}}_{c^\dagger_{\mathbf{k}\tau\bar{\sigma}} d_{j\bar{\sigma}} d_{j\sigma}, d_{l\sigma}}\right], \quad (20)$$

where the occupation number is

$$\langle n_{d_{j\bar{\sigma}}}\rangle = -\frac{1}{\pi}\int_{-D}^0 \text{Im}(\tilde{\mathcal{G}}_{d_{j\bar{\sigma}} d_{j\bar{\sigma}}})d\varepsilon. \quad (21)$$

We employ the Hubbard I approximation [13,25] in order to close this dynamic set of equations for the Green's functions.
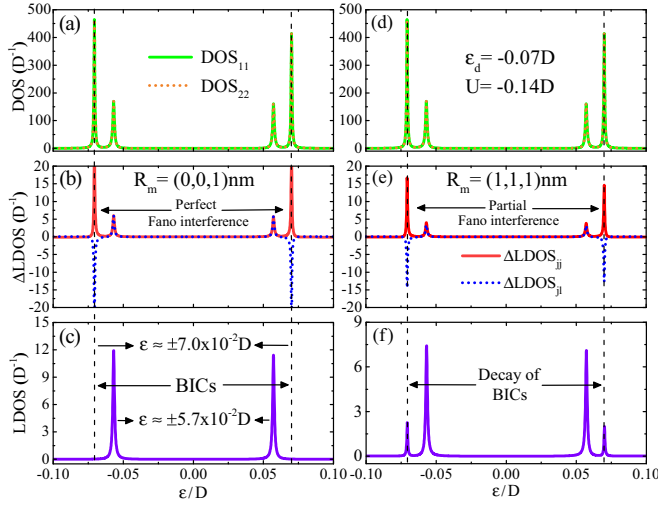
FIG. 2. (a) and (d) The DOS_{11} (solid green curve) and the DOS_{22} (dashed orange curve) of the adatoms. (b) The $\Delta LDOS_{jl}$ profiles at $\mathbf{R}_m = (0,0,1)$ nm, described by Eq. (17), for $j = l$ (solid red curve) and $j \neq l$ (dashed blue curve) where the resonances are canceled perfectly by Fano antiresonances around $\varepsilon \approx \pm 7.0 \times 10^{-2} D$. (c) The total LDOS revealing BICs on the surface of the 3D-DSM host. (e) The $\Delta LDOS_{jl}$ profiles at $\mathbf{R}_m = (1,1,1)$ nm where the destructive interference is not perfect. (f) The total LDOS revealing the decay of BICs at the same energetic positions where BICs are found. The vertical dashed lines crossing the panels indicate the positions where the Fano destructive interference processes occur.

Thereby, we find for the diagonal adatom Green's functions,

$$\tilde{\mathcal{G}}_{d_{j\sigma} d_{j\sigma}} = \frac{\lambda_j^{\bar{\sigma}}}{\varepsilon - \varepsilon_{d_{j\sigma}} - \tilde{\Sigma}_{jj}^{\sigma}}, \qquad (22)$$

where $\lambda_j^{\bar{\sigma}} = 1 + \frac{\langle n_{d_{j\bar{\sigma}}} \rangle U_j}{\varepsilon - \varepsilon_{d_{j\sigma}} - U_j - \Sigma(0)}$ and $\tilde{\Sigma}_{jj}^{\sigma} = \Sigma(0) + \lambda_j^{\bar{\sigma}} \lambda_j^{\bar{\sigma}} \frac{\Sigma(\mathbf{R}_{jj})\Sigma(\mathbf{R}_{jj})}{\varepsilon - \varepsilon_{d_{\bar{j}\sigma}} - \Sigma(0)} = \Sigma(0) + \Sigma_{jj}^{\sigma}$. The mixed Green's functions are as follows:

$$\tilde{\mathcal{G}}_{d_{j\sigma} d_{\bar{j}\sigma}} = \frac{\lambda_j^{\bar{\sigma}} \Sigma(\mathbf{R}_{j\bar{j}})}{\varepsilon - \varepsilon_{d_{j\sigma}} - \Sigma(0)} \tilde{\mathcal{G}}_{d_{j\sigma} d_{\bar{j}\sigma}}. \qquad (23)$$

Results and Discussion. In the following discussion we consider the case of two identical adatoms placed at $\mathbf{R}_{1,2} = (0, \mp 1, 0)$ nm [the surface of the system corresponds to the $(x, y, 1)$-nm plane] with energy levels $\varepsilon_{d_{j\sigma}} = -0.07D$, which are hybridized to the free electrons of the 3D-DSM with strength $v_0 = 0.14D$ and on-site Coulomb repulsion $U_j = 0.14D$. We point out that the change in v_0 just rigidly shifts the profile of the adatom DOS. Additionally, we have chosen $\hbar v_F \approx 5$ eV Å and $D \approx 0.2$ eV, which are experimental parameters for Cd_3As_2 [3,5]. The set of parameters we use corresponds to the symmetric Anderson regime ($2\varepsilon_{d_{j\sigma}} + U_j = 0$). For such conditions the Hamiltonian becomes invariant under particle-hole transformation as can be seen in Fig. 2. The presence of the particle-hole symmetry is in no way necessary for the appearance of the phenomena discussed below.

The four-peak structure in the DOS visible in the upper panels of Fig. 2 emerges from the contributions provided by Coulomb repulsion U_j and interacting self-energy

$\Sigma_{jj}^{\sigma} = \lambda_j^{\bar{\sigma}} \lambda_j^{\bar{\sigma}} \frac{\Sigma(\mathbf{R}_{jj})\Sigma(\mathbf{R}_{jj})}{\varepsilon - \varepsilon_{d_{j\sigma}} - \Sigma(0)}$ in Eq. (22) for the adatoms' Green's functions. The former leads to the formation of the pair of peaks at $\varepsilon_{d_{j\sigma}}$ and $\varepsilon_{d_{j\sigma}} + U_j$ as expected; the latter is responsible for the splitting of both of them. Noteworthy, this self-energy provides effective tunneling between the adatoms mediated by the bulk states of the 3D-DSM, even in the absence of the direct tunneling term $t(\mathbf{R}_{12}) d_{1\sigma}^{\dagger} d_{2\sigma} + $ H.c. This indirect tunneling becomes especially important when adatoms are well separated from each other. This four-peak structure corresponds to the formation of molecular states with remarkable properties: The ground state corresponds to the antibonding configuration. This is a consequence of the particular scaling of the 3D-DSM DOS with energy $\mathcal{D}_0 \propto \varepsilon^2$ entering into the expression for $\Sigma(\mathbf{R}_{mj})$ as a result. If we replace this DOS by the one corresponding to the normal metal the reported effect disappears. Additionally, following Ref. [26] and looking at the poles of the adatoms' Green's function, we recognize $t_{\text{eff}} = \text{Re}[\Sigma(0) + \Sigma_{jj}^{\sigma}]$ as the effective hopping term between the adatoms, which is negative as we have checked it, thus ensuring the antibonding ground state. However, distinctly from Ref. [26] where the negative tunneling term comes from the spin-orbit coupling, here it emerges from Friedel-like oscillations inside the relativistic 3D-DSM environment encoded by the self-energy Σ_{jj}^{σ}.

The nature of the four molecular states can be clarified if one analyzes the corresponding LDOS of the whole system. Note that this quantity is position dependent and its profile on the surface of the system can be visualized experimentally using a STM tip. The middle panels in Fig. 2 illustrate the contribution of the adatoms on the surface LDOS evaluated at $\mathbf{R}_m = (0,0,1)$ nm [Fig. 2(b)] and $\mathbf{R}_m = (1,1,1)$ nm [Fig. 2(e)]. In both panels diagonal terms ($j = l$) present pronounced
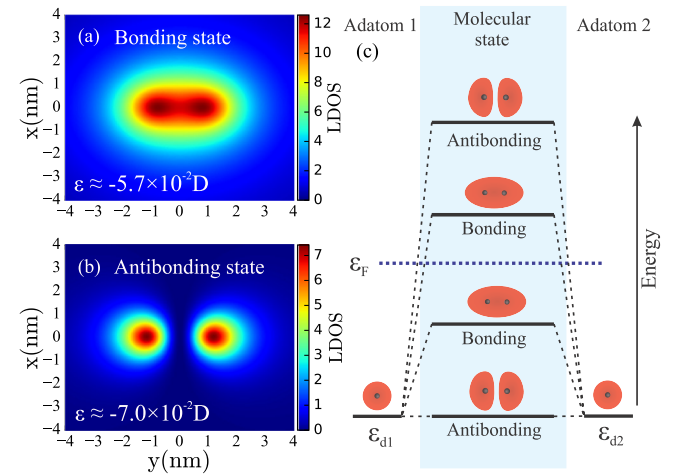

FIG. 3. Topography of the $\Delta LDOS$ on the surface of the 3D-DSM [$\mathbf{R}_m = (x, y, 1)$-nm plane] for two relevant energy values (a) $\varepsilon \approx -5.7 \times 10^{-2} D$ corresponding to the constructive interference of the diagonal and mixed terms in the $\Delta LDOS$. One can clearly see the bonding character of the density profile. (b) $\varepsilon \approx -7.0 \times 10^{-2} D$ corresponding to the destructive interference of the diagonal and mixed terms in the $\Delta LDOS$ for which an antibonding molecular state emerges. Note that this state corresponds to the ground state of the system. (c) A scheme of the hierarchy of the molecular states.
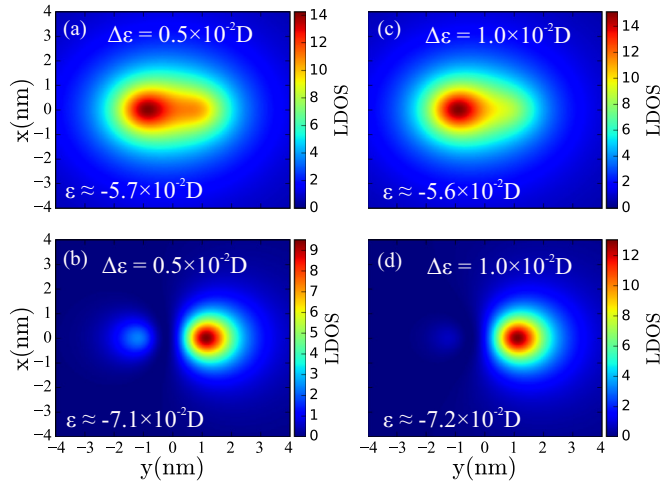
FIG. 4. Topography of the ΔLDOS on the surface of the 3D-DSM [$\mathbf{R}_m = (x,y,1)$-nm plane] illustrating the effects of energy detuning between the adatom levels. Panels (a) and (b) show bonding and antibonding profiles for $\Delta\varepsilon = 0.5 \times 10^{-2}D$ corresponding to the energies $\varepsilon \approx -5.7 \times 10^{-2}D$ and $\varepsilon \approx -7.0 \times 10^{-2}D$, respectively. Panels (c) and (d) show bonding and antibonding profiles for $\Delta\varepsilon = 1.0 \times 10^{-2}D$ corresponding to the energies $\varepsilon \approx -5.6 \times 10^{-2}D$ and $\varepsilon \approx -7.2 \times 10^{-2}D$, respectively.

peaks at the same energies as those of the DOS (upper panels of Fig. 2). The mixed terms ($j \neq l$) show resonances around $\varepsilon \approx \pm 5.7 \times 10^{-2}D$ and antiresonances nearby $\varepsilon \approx \pm 7.0 \times 10^{-2}D$. When one computes the total LDOS as a sum of all contributions from the ΔLDOS_{jl} the interference between diagonal and mixed terms can be constructive or destructive. For the latter case the peaks in the total LDOS become attenuated and can even totally vanish as happens in Fig. 2(c) where only two peaks out of four survive. In this case two peaks disappearing due to Fano destructive interferences [23,24] around $\varepsilon \approx \pm 7.0 \times 10^{-2}D$ correspond to the BICs. Note that full annihilation of the peaks takes place only for certain values of $\mathbf{R}_m$ as one can clearly see in Figs. 2(e) and 2(f). In this case the destructive interference is not perfect, and thus BICs inevitably experience decay into the host continuum.

The profiles of the total LDOS on the 3D-DSM surface [$\mathbf{R}_m = (x,y,1)$-nm plane] are shown in Fig. 3. We considered two distinct values of the energies corresponding to the cases of constructive and destructive Fano interference in the ΔLDOS, (i) $\varepsilon \approx -5.7 \times 10^{-2}D$ and (ii) $\varepsilon \approx -7.0 \times 10^{-2}D$, respectively. For the case of constructive interference shown in Fig. 3(a) the density profile reveals a nodeless covalent molecular state, i.e., a bonding state. On the contrary, when the energy corresponds to destructive Fano interference and the formation of a BIC, the density profile has a pronounced node between the adatoms and thus corresponds to the antibonding state. Note that this latter case corresponds to the peak in the DOS with minimal energy. Thus, different from the case of the real molecules the ground molecular state is antibonding, which is quite remarkable [15]. It is worth mentioning that another pair of bonding and antibonding states exists above the Fermi energy ($\varepsilon_F = 0$) due to the particle-hole symmetry of the original Hamiltonian [Fig. 3(c)].

The molecular states discussed above are robust with respect to the detuning $\Delta\varepsilon$ of the energy levels of the two adatoms. The corresponding profiles of the LDOS for bonding and antibonding states are shown in Fig. 4 for two different values of $\Delta\varepsilon$. Naturally, profiles become asymmetric, but the nodal line between the adatoms revealing the antibonding nature of the ground state remains clearly visible.

Conclusions. To summarize, we evaluated the LDOS on the surface of the 3D-DSM hosting two distant buried adatoms and found that the ground state of this molecular system has a density profile with a node between the atoms and thus corresponds to the antibonding state. This is in contrast with natural molecules for which the ground state is always bonding. The predicted effect appears due to the indirect tunneling between the adatoms mediated by quasirelativistic free electrons of the 3D-DSM.

[1] Z. K. Liu, B. Zhou, Y. Zhang, Z. J. Wang, H. M. Weng, D. Prabhakaran, S.-K. Mo, Z. X. Shen, Z. Fang, X. Dai, Z. Hussain, and Y. L. Chen, Science **343**, 864 (2014).

[2] Z. K. Liu, J. Jiang, B. Zhou, Z. J. Wang, Y. Zhang, H. M. Weng, D. Prabhakaran, S.-K. Mo, H. Peng, P. Dudin, T. Kim, M. Hoesch, Z. Fang, X. Dai, Z. X. Shen, D. L. Feng, Z. Hussain, and Y. L. Chen, Nat. Mater. **13**, 677 (2014).

[3] M. Neupane, S.-Y. Xu, R. Sankar, N. Alidoust, G. Bian, C. Liu, I. Belopolski, T.-R. Chang, H.-T. Jeng, H. Lin, A. Bansil, F. Chou, and M. Z. Hasan, Nat. Commun. **5**, 3786 (2014).

[4] S.-Y. Xu, C. Liu, S. K. Kushwaha, R. Sankar, J. W. Krizan, I. Belopolski, M. Neupane, G. Bian, N. Alidoust, T.-R. Chang, H.-T. Jeng, C.-Y. Huang, W.-F. Tsai, H. Lin, P. P. Shibayev, F.-C. Chou, R. J. Cava, and M. Z. Hasan, Science **347**, 294 (2015).

[5] S. Borisenko, Q. Gibson, D. Evtushinsky, V. Zabolotnyy, B. Büchner, and R. J. Cava, Phys. Rev. Lett. **113**, 027603 (2014).

[6] K. S. Novoselov, Rev. Mod. Phys. **83**, 837 (2011).

[7] N. M. R. Peres, Rev. Mod. Phys. **82**, 2673 (2010).

[8] A. H. Castro Neto, F. Guinea, N. M. R. Peres, K. S. Novoselov, and A. K. Geim, Rev. Mod. Phys. **81**, 109 (2009).

[9] J. Feng, Y. Pang, D. Wu, Z. Wang, H. Weng, J. Li, X. Dai, Z. Fang, Y. Shi, and L. Lu, Phys. Rev. B **92**, 081306(R) (2015).

[10] P. J. W. Moll, N. L. Nair, T. Helm, A. C. Potter, I. Kimchi, A. Vishwanath, and J. G. Analytis, Nature (London) **535**, 266 (2016).

[11] T. Liang, Q. Gibson, M. N. Ali, M. Liu, R. J. Cava, and N. P. Ong, Nat. Mater. **14**, 280 (2014).

[12] C. W. Hsu, B. Zhen, A. D. Stone, J. D. Joannopoulos, and M. Soljacic, Nat. Rev. Mater. **1**, 16048 (2016).

[13] L. H. Guessi, R. S. Machado, Y. Marques, L. S. Ricco, K. Kristinsson, M. Yoshida, I. A. Shelykh, M. de Souza, and A. C. Seridonio, Phys. Rev. B **92**, 045409 (2015).

[14] L. H. Guessi, Y. Marques, R. S. Machado, K. Kristinsson, L. S. Ricco, I. A. Shelykh, M. S. Figueira, M. de Souza, and A. C. Seridonio, Phys. Rev. B **92**, 245107 (2015).

[15] M. F. Doty, J. I. Climente, M. Korkusinski, M. Scheibner, A. S. Bracker, P. Hawrylak, and D. Gammon, Phys. Rev. Lett. **102**, 047401 (2009).

[16] A. I. Yakimov, V. A. Timofeev, A. I. Nikiforov, and A. V. Dvurechenskii, JETP Lett. **94**, 744 (2011).

[17] G. Reecht, B. Heinrich, H. Bulou, F. Scheurer, L. Limot, and G. Schull, arXiv:1703.05622.

[18] P. W. Anderson, Phys. Rev. **124**, 41 (1961).

[19] H.-R. Chang, J. Zhou, S.-X. Wang, W.-Y. Shan, and D. Xiao, Phys. Rev. B **92**, 241103(R) (2015).

[20] M. V. Hosseini and M. Askari, Phys. Rev. B **92**, 224435 (2015).

[21] H. Haug and A. P. Jauho, *Quantum Kinetics in Transport and Optics of Semiconductors*, Springer Series in Solid-State Sciences Vol. 123 (Springer, New York, 1996).

[22] A. Principi, G. Vignale, and E. Rossi, Phys. Rev. B **92**, 041107(R) (2015).

[23] U. Fano, Phys. Rev. **124**, 1866 (1961).

[24] A. E. Miroshnichenko, S. Flach, and Y. S. Kivshar, Rev. Mod. Phys. **82**, 2257 (2010).

[25] J. Hubbard, Proc. R. Soc. London, Ser. A **281**, 401 (1964).

[26] J. I. Climente, M. Korkusinski, G. Goldoni, and P. Hawrylak, Phys. Rev. B **78**, 115323 (2008).